Journal of Applied Mechanics and Technical Physics, Vol. 42, No. 6, pp. 949–958, 2001

EXPLOSION WITH PLASMA QUASITRAPPING IN A DIPOLE FIELD

V. M. Antonov,[1] Yu. P. Zakharov,[1] A. V. Melekhov,[1]
V. N. Oraevskii,[2] A. G. Ponomarenko,[1] and V. G. Posukh[1]

UDC 533.95

Experiments using a powerful CO_2 *amplifier were performed with the aim of developing a technique for simulating a space explosion in the magnetosphere of the Earth and other planets under laboratory conditions using laser plasma clouds. The amplifier radiation with an energy of about* 300 J *and a pulse duration of about* 10^{-7} sec *focused on a Caprolon target of* 4 mm *diameter produced an exploding plasma in a dipole magnetic field with a characteristic dimension of* 15 cm *and a magnetic moment of* $1.1 \cdot 10^7$ Gs $\cdot$ cm^3. *The paper presents preliminary results of simulating a space explosion under quasitrapping conditions, where the energy of the explosion is much lower than the geomagnetic energy and the explosion point is located in the equatorial plane at a distance of two Earth's radii.*

Introduction. The problem of plasma quasitrapping in a dipole magnetic field with external injection of the type of a point explosion arose during the first space tests of nuclear weapons ("Argus," "Starfish," etc.) [1, 2].

Because of the nuclear test ban, researchers has begun space experiments with plasma injection using electrical, chemical, and solar energies (AMPTE, Crest, et al.) [3]. The low energy of explosions restricts the potentials of these experiments to solving some particular, though rather important problems, such as investigation of the stability of the plasma boundary, the structure of collisionless shock waves during interaction with the "solar wind," acceleration of particles, etc. Most of these problems are successfully solved in laboratory experiments, which greatly reduces financial expenditures [4, 5]. Thus, simulations of strong explosions with plasma deceleration radius comparable to the dimensions of the dipole or even the magnetospheres of planets or stars, are now feasible only under laboratory conditions.

Practical problems in similar formulation arise during direct production of electrical energy in a magnetic trap in laser fusion synthesis and in designing a laser-driven rocket engine.

In connection with the development of the program "Space Weather," of considerable interest are model tests of the global stability of the magnetosphere against strong perturbations in the "solar wind" or experiments using nuclear charges to break asteroids [6].

The present papers describes a model experiment on external (explosive) injection of a plasma in the quasitrapping mode, i.e., under conditions where the explosion energy is much lower than the energy of the magnetic field of the magnetosphere (for example, of the Earth) and the characteristic scales of interaction are comparable to the dimensions of the planet.

1. Formulation of the Problem and Similarity Parameters. In studying the effects of external injection, we consider only explosions whose plasma products have initial expansion velocity V_0 of the order of or less than the velocity of Alfvén waves in the environment, i.e., $V_0 \leqslant V_A$, which corresponds to the case of small initial Alfvén–Mach numbers $M_A = V_0/V_A \leqslant 1$. These conditions hold for explosions at a distance of $L = R_0/R_g \geqslant 1.5$ if $V_0 \leqslant (0.5\text{–}1) \cdot 10^8$ cm/sec. Here R_0 is the distance from the center of the dipole to the explosion point and R_g is the dipole surface radius (for example, the radius of the conducting surface of the ionosphere or the Earth's surface).

[1]Institute of Laser Physics, Siberian Division, Russian Academy of Sciences, Novosibirsk 630090; [2]Institute of Geomagnetism, Ionosphere, and Radiowave Propagation, Russian Academy of Sciences, Moscow 142190. Translated from Prikladnaya Mekhanika i Tekhnicheskaya Fizika, Vol. 42, No. 6, pp. 27–38, November–December, 2001. Original article submitted May 28, 2001.

0021-8944/01/4206-0949 $25.00

In the case considered, it is possible to neglect the interaction of the hot plasma with the background plasma and to take into account as a first approximation only its interaction with the dipole magnetic field [6].

In the collisionless case, the process is characterized by the following dimensionless parameters (complexes):

$$æ = \left(\frac{R_B}{R_0}\right)^3 = E_0\,\frac{3}{\mu_g B_g}\,L^3, \quad \varepsilon_B = \frac{R_L}{R_B}, \quad L = \frac{R_0}{R_g}, \quad \theta, \quad \frac{m_\mathrm{i}}{z_\mathrm{i} m_\mathrm{e}} \gg 1, \quad \frac{V_0}{c} \ll 1.$$

Here $R_L = m_\mathrm{i} c V_0/(z_\mathrm{i} e B_0)$ is the cyclotron radius of ions of the cloud at the explosion point R_0, V_0 is the initial velocity of ions of the cloud, B_0 is the magnitude of the magnetic field at the explosion point, c is the velocity of light, m_i and m_e are the ion and electron masses, respectively, z_i is the ion charge, E_0 is the explosion energy, $\mu_g B_g/3$ is the energy of the magnetic sphere, and $R_B = (3E_0/B_0^2)^{1/3}$ is the characteristic scale of plasma deceleration in a homogeneous magnetic field $B = B_0$. In the ideal MHD approximation ($\varepsilon_B \ll 1$), the parameter æ characterizes the shape and dimensions of the magnetic cavity, which should also depend on the latitudinal angle θ. In a more general case, the parameter ε_B can be arbitrary, and its effect on the plasma flow pattern in a dipole field requires experimental test. From a theoretical viewpoint, this question has not been adequately studied even for explosions in a homogeneous field [7].

Experiments performed on the KI-1 facility [8] showed that an increase of the parameter ε_B ($\varepsilon_B > 1$) enhances the flutter mode on the magnetic cavity boundary, which leads to substantial weakening of plasma deceleration by the magnetic field and reduction in cavity dimensions ($R < R_B$). The plasma breaks up into separate jets with characteristic dimension not exceeding the value of $R_L/4$, polarizes, and flows out of the cavity across the field without energy losses. This means that there is a considerable reduction in plasma trapping efficiency with an initial value $\beta = n_{i(0)} m_\mathrm{i} V_0^2 4\pi/B_0^2 \gg 1$ in a homogeneous magnetic field [$n_\mathrm{i}(0)$ is the ion concentration at the moment of laser plasma generation].

Experiments with an inhomogeneous magnetic field, in particular, a dipole magnetic field, similar to those first performed on the KI-1 facility [9], showed that the theoretical model of [4], based on the MHD-approximation, adequately describes plasma motion and the formation of a magnetic cavity only at the initial stage of deceleration. Similar results were obtained by comparison of data from the KÉVL-1 experiment with results of three-dimensional numerical calculations [10].

Thus, there is an obvious need to perform further experiments to refine or develop appropriate theoretical models and calculations.

2. Description of the KI-1 Facility. The KI-1 facility was designed to simulate nonstationary processes in space plasmas under laboratory conditions. As a rule, phenomena are considered that are presently difficult or impossible to study using space vehicles [9, 11].

The facility incorporates a high-vacuum (about 10^{-5} Pa) chamber of 1.25 m diameter and 5 m length, a powerful CO_2 amplifier with an energy of 10^3 J and a pulse duration of 10^{-7} sec, a quasistationary axial magnetic field $B \leqslant 1$ kGs, and a pulse magnetic dipole with a magnetic moment $\mu \approx 10^7$ Gs$\cdot$ cm^3. In addition, to model the "solar wind" there is a hydrogen plasma source capable of producing artificial magnetosphere conditions or filling the chamber with a magnetized background plasma of concentration $n_\mathrm{i} \sim 10^{12}$–$10^{14}$ cm^{-3} within 10^{-3}–10^{-4} sec.

A space explosion is simulated using two colliding laser beams with an intensity of about 10^{10} W/cm^2, which are focused on a 4 mm diameter sphere made of Caprolon $(C_6H_4ON)_n$ or other materials fixed on a thin thread of 0.2 mm diameter. At the location of the sphere, the diameter of the beams ia approximately 10 mm. Under these conditions, it is possible to produce a quasispherical cloud of a laser plasma which consists basically of C^{+4}, C^{+3}, and N^+ ions scattering with a radial velocity of $(1\text{–}2)\cdot 10^7$ cm/sec.

Figure 1 shows photographs of the luminescence of a Caprolon laser plasma, taken with the use of an image device in a time of about 30 nsec. The boundary of the luminescence of the cloud from each of the beams is reminiscent of a cardioid. Therefore, under the same irradiation conditions, it is possible to obtain a quasispherical cloud with a ratio of the axes of 1.2–1.5.

3. Diagnostic Methods. In studying the dynamics of laser plasma motion and measuring plasma parameters, we used the following diagnostic means and methods (Fig. 2):

— High-velocity photorecording with an exposure of less than 30 nsec in separate lines of multiply charged ions of the laser plasma or in the integral luminescence in the optical range;

— Measuring the plasma particle concentration using double cylindrical Langmuir probes with a spherical directional pattern;

— Diagnostics of local flows of the ion charge by surface probes and Faraday cylinders;

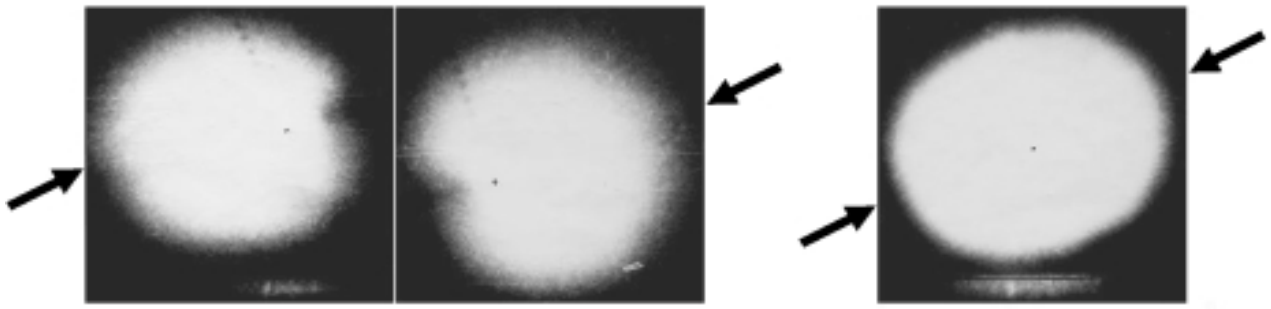

Fig. 1. Luminescence of a Caprolon plasma under one and two-beam irradiation 0.8 μsec after the beginning of the explosion (arrows show the directions of the laser beam; scale 1 : 6.4).

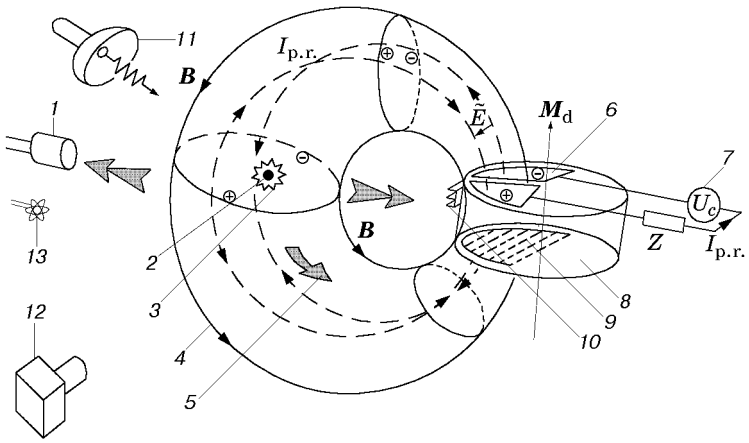

Fig. 2. Diagram of plasma motion and diagnostic equipment: 1) modified Langmuir probes (Faraday cylinders); 2) target; 3) expanding plasma cloud; 4) unperturbed magnetic lines of force; 5) plasma flows; 6) electrodes in the polar region; 7) external voltage source; 8) magnetic field generator; 9) segmented calorimeter in the polar region; 10) equatorial calorimeter; 11) microwave locator (35 GHz); 12) image device; 13) array of five three-component magnetic probes; $\tilde{E}$ and $I_{p.r.}$ are the large-scale e.m.f. and currents on the dipole surface in the polar region, respectively, Z is the load impedance, and $\boldsymbol{M}_d$ is the magnetic dipole moment.

— Determining the initial charge–mass composition of the laser plasma ions by a time-of-flight analyzer with preliminary ion acceleration;

— Determining the dynamics of motion of a plasmoid layer with an electron concentration $n_e = 1.5{\cdot}10^{13}$ cm^{-3} by a phase locator at a frequency of 35 GHz;

— Recording magnetic field perturbations by a three-coordinate miniature magnetic probes;

— Measuring the integral energy of the plasma reaching the equatorial region on the dipole surface by a thermocouple calorimeter;

— Measuring the integral plasma energy released on the dipole surface in the range of latitudes of 35–83° by a latitude-segmented calorimeter;

— Recording large-scale currents, potentials, and particle flows appearing in the polar regions by two conducting plate electrodes placed in the polar region.

The diagnostic equipment provided for local spatial and temporal resolutions of not less than 0.5 cm and 20 nsec, respectively.

Special systems for fastening and moving the electrical and magnetic probes were used to study the of dynamics of plasma expansion in the equatorial and meridional planes. Placement of the probes in the radial direction from the target made it possible to determine the character of the expansion and to calculate the initial parameters of the plasma cloud such as the total kinetic energy E_0, the total number of ions N_i, etc.

The contact diagnostic equipment operated in a "floating" mode. Signals from the probes were transmitted using broad-band pulse transformers and image converters.

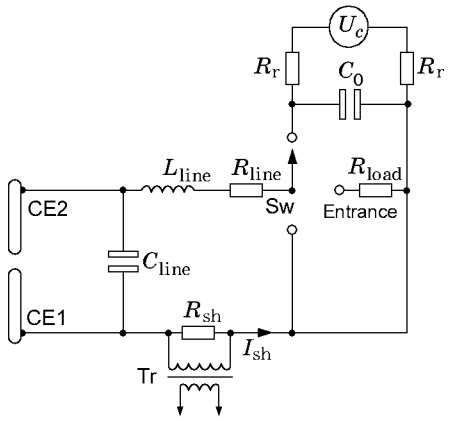

Fig. 3. Diagram of measurements of currents and potentials in the polar region: CE1 and CE2 are current electrodes, I_{sh} is the measuring circuit current, U_c is the external e.m.f. voltage, $L_{line} = 1.6 \cdot 10^{-7}$ H, $C_{line} = 800$ pF, and $R_{line} = 0.04$ Ω are the inductance, capacitance, and resistance of the transmission line, respectively, $R_{sh} = 0.04$ Ω is an ohmic shunt for measuring the current $I_{p.r.}$, Tr is an isolating broad-band transformer (0.001–50 MHz), Sw is a measurement mode switch, $R_r = 30$ kΩ are high-resistance resistors, $R_{load} = 20$–50 Ω is a load resistor for measurements of the potential difference $U_{p.r.}$, and $C_0 = 600$ μF is the capacitance of the external voltage source.

The systems for supplying a potential difference and measuring the current between the probe electrodes had a high-resistance galvanic isolation from the conducting elements of the facility, based on broad-band transformers and optoelectronic couples (light-emitting diode–photo diode) with a passband of not less than 20 MHz.

A diagram of the measurements of currents and potentials in the polar region is given in Fig. 3. Two current-receiving plate titanium electrodes 50 μm thick were placed on the side of the south pole. The dimensions of the electrodes provided for monitoring of all particles that reached the dipole surfaces and moved toward the pole from the magnetic latitude of the target and upward. Along the main meridional plane between the electrodes there was a clearance $h = 0.3$ cm $\gg R_{L,e}$ ($R_{L,e}$ is the Larmor electron radius).

A flexible line transmitted the electrode current and voltage to the measuring circuit located outside the vacuum chamber. The interelectrode circuit current I_{sh} was measured by a shunt ($R_{sh} = 0.04$ Ω) connected to the recording equipment with the interposition of an isolating transformer Tr. In the current measurement mode, the transmission line was connected directly to the shunt. In this case, the circuit had minimum introduced impedance and $I_{p.r.} = I_{sh}$ (the subscript p.r. denotes values in the polar region).

For measurements of potentials, a high-resistance resistor $R_{load} = 20$–50 Ω was switched into the circuit of the current I_{sh}. The amplitude of the interelectrode potential difference was calculated by the relation $U_{p.r.} = I_{sh}R_{load}$ (the measurement mode switch was in the position Sw–Entrance).

The external voltage source U_c based on the capacitor C_0 was switched into the circuit to refine the ion saturation current and determine the symmetry of the plasma flows to the electrodes. In measurements of the ion saturation current, an additional negative bias voltage $U_c \approx U_{p.r.}$ was applied to the electrode CE1 (to the west of the main meridional plane).

The total number of ions reaching the electrodes was calculated from the measurement data by the formula

$$N_{p.r.} = \frac{2}{e\langle z_i\rangle(1+k)} \int_0^t I_{p.r.}\, dt,$$

where $k = 0.7$ and $\langle z_i\rangle = 2.7$ are the secondary emission coefficients and the ion charge, respectively, measured by the probes.

4. Experimental Conditions. According to the theoretical estimates of [4], the present experiments in the quasitrapping mode were performed under the following conditions:

— An explosion is carried out in the equatorial plane because in this case, smaller values of $æ$ are needed to implement the trapping mode and the plasma dynamics can be studied in the polar region.

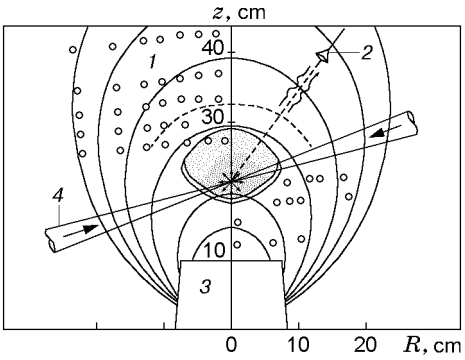

Fig. 4. Diagram of experiment: 1) cylindrical zones; 2) locator; 3) magnetic dipole; 4) laser beam (10.6 μm); points are the locations of the probes.

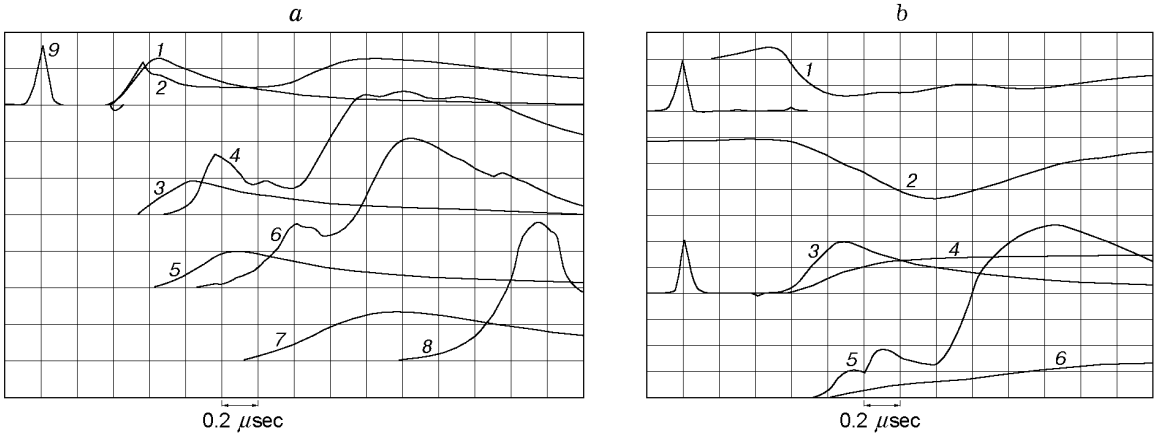

Fig. 5. Oscillograms of Langmuir probes placed in the upper half-plane (a) and readings of a magnetic probe located at an angle of 41.5° ($r = 6.5$ cm) and a Langmuir probe ($z = 9$ cm) (b): (a) curves 1, 3, 5, and 7 refer to $B_0 = 0$ (9 is a laser pulse), curves 2, 4, 6, and 8 refer to $B_0 = 1$ kGs for $z = 6.5$ (1 and 2), 9 (3 and 4), 12 (5 and 6), and 21.8 cm (7 and 8); scale factors $n_\text{i} = 5 \cdot 10^{13}$ (1), 10^{14} (2), $2 \cdot 10^{13}$ (3 and 4), 10^{13} (5 and 6), 10^{12} (7), and $5 \cdot 10^{12}$ cm^{-3} (8); (b) curve 1 refers to $M(t)$ and curve 2 to the rotation angle α of the resulting vector $\boldsymbol{B}$, curves 3 and 5 to $n_\text{i}(t)$, and curves 4 and 6 to $\varepsilon(t)$; scale factors: for curve 1, $M = 0.5$, for curve 2, $\alpha = 50°$, for curves 3 and 5, $n_\text{i} = 2 \cdot 10^{13}$ cm^{-3}, and for curves 4 and 6, $\varepsilon = 0.4$ J/ster.

— Taking into account the possibilities of the diagnostic equipment, we chose the geometry of the experiments and the mode of producing a laser cloud with the following parameters: $\bar{E}_0 = 8$ J, composition of the cloud $(1/2)\text{C}_4^{+4}$, $(1/2)\text{H}^+$, average mass of ions of the cloud $\bar{m}_\text{i} = 6.5$, average ion charge $\bar{z}_\text{i} = 2.5$, average ion velocity $\bar{V}_0 = 1.5 \cdot 10^7$ cm/sec, total number of ions $N_\text{i} \approx 6.6 \cdot 10^{16}$, magnetic field at the explosion point $B_0(R_0) = 10^3$ Gs, characteristic deceleration radius $R_B = 6.2$ cm, characteristic time of plasma deceleration $t_B = R_B/V_0 = 4.13 \cdot 10^{-7}$ sec $\gg t_n = 10^{-7}$ sec (t_n is the laser pulse duration), characteristic Larmor radius $\bar{R}_L \approx 3.9$ cm, distance to the explosion point $R_0 = 21.8$ cm, and characteristic dimension of the dipole shell $R_g = 10$ cm.

The experimental conditions ensured the following values of the dimensionless complexes: $æ = 2 \cdot 10^{-2}$, $\varepsilon_B \approx 0.62$, $L \approx 2.18$, and $V_0/c \ll 1$.

5. Experimental Results. In the present experiments, it was planned to investigate the flow pattern of the plasma produced by explosion of a target located in the equatorial plane at a distance $L = R_0/R_g = 2.18$, where R_0 is the distance from the center of the dipole to the target, and R_g is the characteristic dimension of the external shell of the dipole, whose shape and material can be different (stainless steel, titanium, copper, dielectric, etc.).

Since the experiments described here were performed for the first time and had a methodical nature, the ionosphere in the polar regions was simulated using a titanium foil.

A diagram of the experiments is shown in Fig. 4.

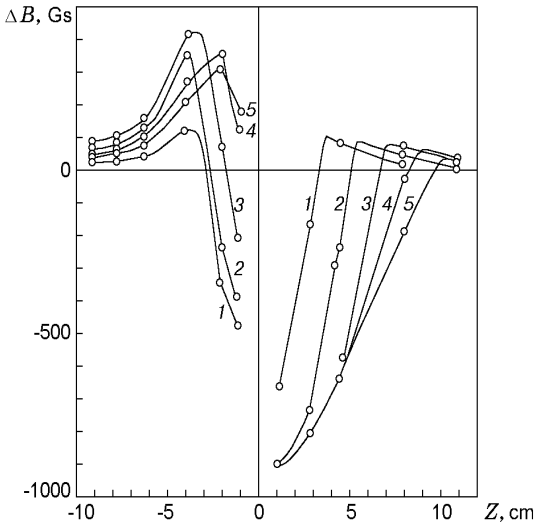

Fig. 6. Spatial–temporal distribution of magnetic-field perturbations $\Delta \boldsymbol{B}$ in the "dipole–target" direction for $t = 0.2$ (1), 0.4 (2), 0.6 (3), 0.8 (4), and 1.0 μsec (5).

Figure 5a gives typical oscillograms of Langmuir probes placed in the upper half-plane at various distances from the center along the z axis (see Fig. 4). The oscillograms show the shapes of the observed signals for free expansion of the cloud with and without the dipole field. The amplitudes of the signals are proportional to the ion concentration n_{i}. The delay of these signals relative to each other suggests that there is substantial deceleration of the cloud during its motion across the magnetic field. The magnetic probe located at the same distance as the Langmuir probe nearest to the target ($z = 6.5$ cm) shows the stage of formation of a magnetic cavity characterized by fast "sweeping-out" of the initial magnetic field $B_0(r)$. The efficiency of this process is determined by the relative value of the magnitude of the perturbed magnetic field $M(r,t) = |\boldsymbol{B}|/|\boldsymbol{B}_0| = \sqrt{(\boldsymbol{B}_0 + \Delta\boldsymbol{B})^2/\boldsymbol{B}_0^2}$, where $\Delta \boldsymbol{B}$ is the field produced by diamagnetic currents at the plasma boundary. Figure 5b shows a curve of $M(t)$ (curve 1) calculated from measurements of values of $\Delta \boldsymbol{B}$ using a three-component magnetic probe located at the point $z = 6.5$ cm (see Fig. 4). From the oscillograms it follows that ahead of the expanding plasma front, the magnetic field increases ($M > 1$) and then decreases sharply, reaching the value of $M \approx 0.25$, which is indicative of a strong reduction in plasma magnetic field, i.e., the formation of a magnetic cavity.

The stage of deceleration, i.e., quasitrapping, is seen most vividly in the oscillogram taken with the Langmuir probe located on the vertical axis at a distance from the target $z \approx 9$ cm (curves 3–6 in Fig. 5b). It is evident that the relative losses of energy by the cloud in this direction, which characterize the trapping efficiency, are $\eta = (\varepsilon(0) - \varepsilon(B))/\varepsilon(0) \leqslant 60\%$ which is close to the theoretical value $\eta \approx 75\%$ (ε is the energy supplied to the probe).

By the moment $t \leqslant 0.5$ μsec, the probes established in the lower hemisphere along the vertical axis (see Fig. 4) detect complete stop of the plasma in the direction to the dipole at a distance of up to 5 cm and subsequent plasma reflection to the upper hemisphere.

Figure 6 gives the spatial distribution of the magnetic cavity along the vertical axis at various times, which agrees satisfactorily with the measurements by electrical probes.

Thus, the duration of the quasitrapping stage is $\Delta t \approx 1.0$–1.2 μsec, and in the equatorial plane, the cross-sectional dimensions of the cloud and the magnetic cavity approach theoretical values.

In Fig. 7 it is evident that with time, the plasma luminescence region in the meridional plane acquires a distinct boundary in the lower hemisphere, a quasispherical boundary in the upper hemisphere, and an elongated boundary in the direction of the magnetic poles of two conical jets. The surface of these jets nearest to the dipole "is connected" to the plasma in the lower hemisphere, and the external surface to the plasma in the upper hemisphere. This picture resembles the "horns" in the polar region of the Earth into which the "solar wind" flows.

5.1. *Structuring of Plasma.* The photographs and signals recording the arrival of the plasma at the polar region show the occurrence of bright luminous spots, which are asymmetric about the meridional section, and occurrence of currents passing in the foil in the west–east direction.

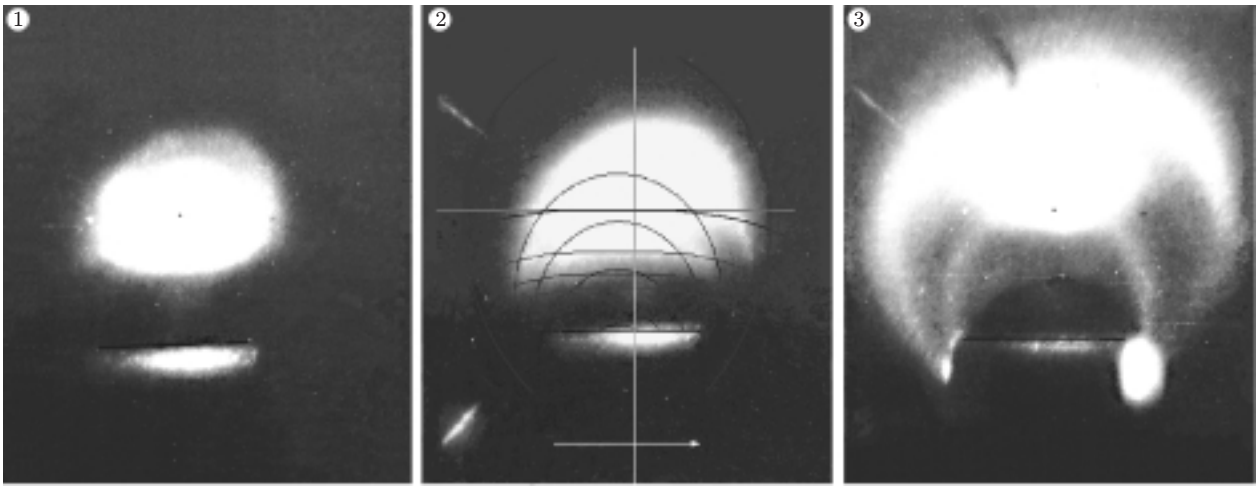

Fig. 7. Luminescence of the plasma in the meridional plane (scale 1 : 6.8; exposure 30 nsec) for $t = 0.7$ (1), 1.0 (2), and 1.65 μsec (3); the horizontal luminous strip at the bottom of the frames is the reflected light from the dipole surface.

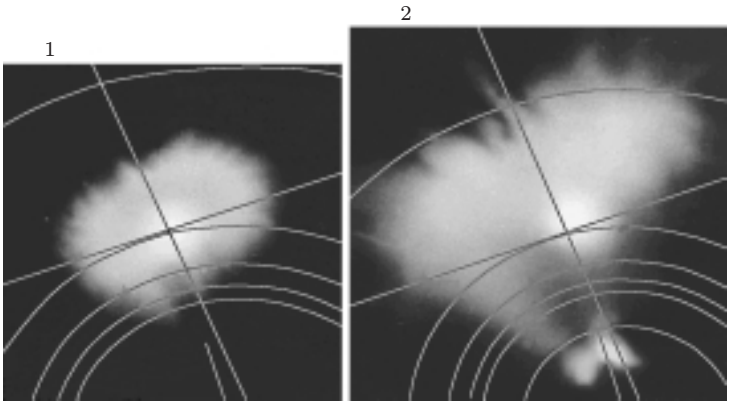

Fig. 8

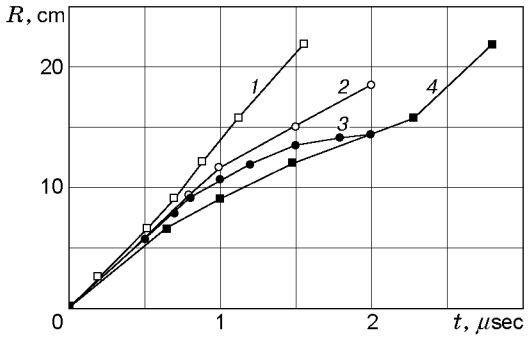

Fig. 9

Fig. 8. Photographs taken with the use of an image device in a direction perpendicular to the equatorial plane for $t = 0.95$ (frame 1; scale 1 : 6.28) and 2.4 μsec (frame 2; scale 1 : 8).

Fig. 9. (R–t) diagram of the motion of the upper boundary of the plasma cloud: 1) position of the ion density front at the leading edge of the cloud for $B_0 = 0$; 2) motion of the microwave radiation front; 3) MHD calculations in a sector approximation [4]; 4) maximum ion density in the magnetic field.

Apparently, the spots results from the development of unipolar arcs which ensure shorting of the longitudinal currents in the artificial ionosphere. These spots are clearly distinguished against the background of the general diffuse luminescence, whose shape reflects the projection (along the force lines) of the equatorial section of the plasma onto the polar region. The indicated phenomena develop intensely at the end of the deceleration stage, which at $t \geqslant 1$ μsec grades into the stage of fast developing necks on the external plasma boundary.

The picture described above is well illustrated by the photographs in Fig. 8 taken using an image device in a direction perpendicular to the equatorial plane at two times. In the interval $\Delta t = 1$–2 μsec, the number of modes decreases from $m \approx 30$ to $m \approx 5$–7, i.e., the plasma breaks up into separate tubes, each of which moves independently away from the dipole with a speed $V = (6\text{–}8) \cdot 10^6$ cm/sec $< V_0$.

In the present experiments, simultaneous photorecording of the plasma luminescence in two perpendicular directions was not possible. Therefore, the dipole was rotated through 90°, i.e., the direction of beam incidence relative to the direction of the magnetic field line at the explosion point was changed.

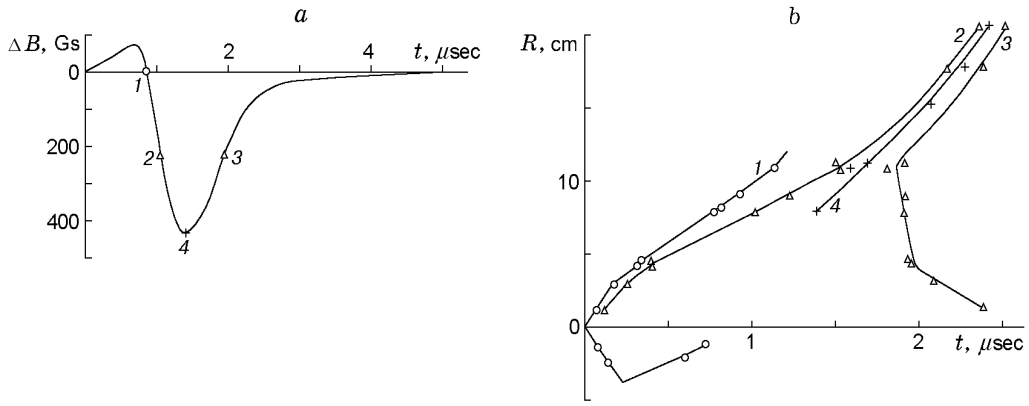

Fig. 10. Typical oscillogram of magnetic-field perturbation (a) and (R–t) diagram (b): point 1 is the beginning of a magnetic cavity, points 2 and 3 are its leading and trailing edges, and point 4 is the maximum of the displaced field.

In Fig. 7, the laser beams are located in the meridional plane, and in Fig. 8, they are located in the equatorial plane. In the first case, at the stage of development of the flutter mode, detected by electrical probes, a smaller number of modes was observed, and at the third stage, just one mode was observed, which was projected into the polar region as a single jet (frame 3 in Fig. 7).

Results of the measurements performed give a more detailed plasma flow pattern in the present experiments.

Figures 9 and 10 show (R–t) diagrams of the motion of the external plasma boundary obtained by probes and methods of microwave location, motion of the front of the magnetic cavity, and plasma motion in the absence of a magnetic field. The data were obtained under conditions of passage of a laser beam in the meridional plane. One can clearly see the development of the first stage, where the energy of the cloud is transferred to the magnetic field and the motion of the boundary slows down. Thus, the radius of the cloud tends to the maximum possible theoretical value of the deceleration radius in the upper hemisphere.

The magnetic cavity boundary lags behind the plasma boundary more strongly, which indicates that the flutter mode begins to influence the magnetic deceleration efficiency. As was noted above, a similar picture was observed in a homogeneous magnetic field, too [5, 7]. This means that the magnetic field inhomogeneity $\Delta R \simeq R_0/3 \sim R_B$ does not suppress the development of the flutter mode under conditions of the present experiment.

When the laser beam is in the meridional plane, the plasma, beginning at the distance $r \approx R_B$, enters a one-mode regime, compresses in the equatorial direction, and accelerates as a diamagnetic jet in the radial direction with a velocity $V \approx (5\text{–}8) \cdot 10^6$ cm/sec, as can be clearly seen in all (R–t) diagrams and photographs.

5.2. *Results of Measurements in the Polar Region.* The dynamics of formation of currents and potentials in the polar region is illustrated in Fig. 11, which shows typical oscillograms of the current $I_{\text{p.r.}}$ and the potential difference $U_{\text{p.r.}}$ at $B_0 = 1.0$ and 0.5 kGs. The direction of the current $I_{\text{p.r.}}$ corresponds to the motion of the positive charge along the measuring circuit from the electrode CE1 (western longitude) to the electrode CE2. An analysis of the potential difference confirms that the positive charge of the electrode CE1 is higher. The recorded signals of $U_{\text{p.r.}}$ and $I_{\text{p.r.}}$ appear with a delay $t \approx 0.5$ μsec from the moment of a laser pulse irradiation of the target.

Probe measurements in the equatorial plane show that beginning with $t \approx 0.5$ μsec, the "cavity" with completely displaced magnetic field and the plasmoid move ion the direction from the dipole toward smaller fields. Apparently, the recorded potential difference $U_{\text{p.r.}}$ suggests the occurrence of electrical fields during plasmoid motion across the magnetic field lines and subsequent "transfer" of them to the dipole surface along the magnetic field lines.

Contact of the plasma with the conducting dipole surface gives rise to current. The charge from the positively charged tubes is transferred by the ion flow from the plasma, and the charge from negatively charged tubes is transferred by the electron flow. The maximum value of the current $I_{\text{p.r.}}$ was limited by the ion current to the surface of the electrodes and did not exceed 0.05 of the total surface current of the plasmoid at the strongly diamagnetic stage (before 1.5 μsec) or directional ion flow at later time.

The greatest energy release in the polar region occurs at times $t \approx 1\text{–}3$ μsec, when a considerable portion of the energy of the displaced magnetic field is again converted to the kinetic energy of plasma flows.

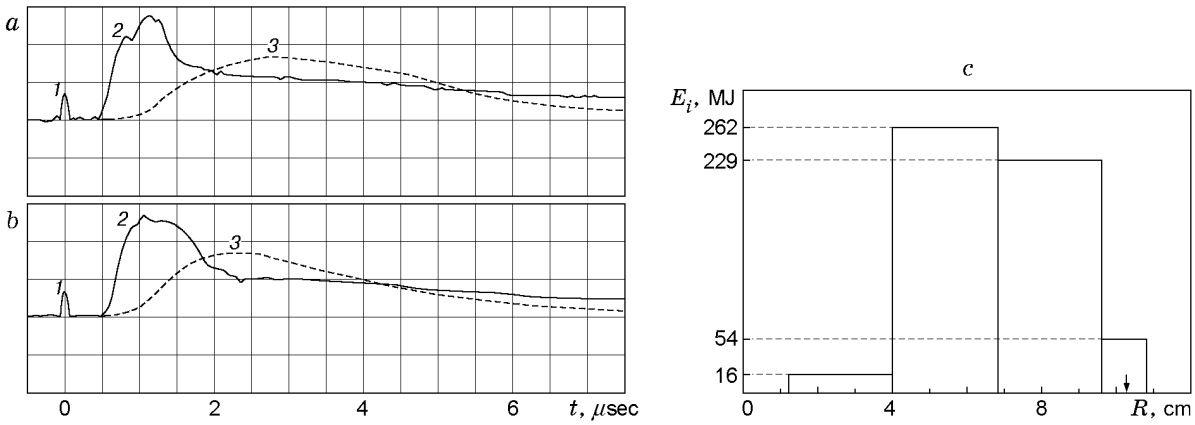

Fig. 11. Distribution of the potential difference $U_{\text{p.r.}}$ (a), current $I_{\text{p.r.}}$ (b), and energy (c) in the polar region (the arrow shows the edge of the face surface of the dipole body): 1) laser pulse; 2) $U_{\text{p.r.}}$ (scale factor 113 V); 3) $I_{\text{p.r.}}$ (scale factor 192 A); $B_0 = 1.0$ (a) and 0.5 kGs (b).

TABLE 1

B_0, kGs	$U^{\max}_{\text{p.r.}}$, V		$I^{\max}_{\text{p.r.}}$, A		$U^{*}_{\text{p.r.}}$, V		$N_{\text{p.r.}} \cdot 10^{-15}$		$E_{\text{p.r.}}$, J	
	MP	EP	MP	EP	MP	EP	MP	EP	MP	EP
1.0	333	511	630	719	135	184	7.5	6.16	0.542	0.458
0.5	281	359	578	520	111	154	4.9	5.19	0.324	0.311
0.25	107	187	580	308	58	78.3	4.6	2.25	0.153	0.085
0.1	49.5	59	423	139	32	39.5	4.4	1.29	0.045	0.005
0	0	—	0	—	0	—	—	—	0	—

Note. MP is the meridional plane and EP is the equatorial plane.

The integral energy distribution along the dipole surface is presented in Fig. 11c. From these data it follows that approximately half of the recorded energy is supplied from the plasma quasitrapping region (lower plasma jet). The other half of the energy is transferred to higher latitudes from the particles of the receding plasmoid.

The energy of the polar calorimeter and the potential difference increase with magnetic field amplification, showing a tendency toward saturation at $B_0 \approx 1$ kGs. The maximum recorded energy did not exceed the value of $0.125E_0$ (E_0 is the initial energy of the plasma cloud).

An analysis of measurement data shows that factor of conversion of kinetic and electrical energy to the energy measured by the calorimeter can differ from unity and be of the order of 0.5 (secondary plasma and intense radiation from the contact area are recorded). Therefore, it is necessary to update the diagnostic equipment and develop recording procedures that differentiate between the kinetic and electrical components of the absorbed energy.

Table 1 lists experimental data on the averaged currents, potentials, and flows of particles and energy in the polar region ($U^{\max}_{\text{p.r.}}$ is the maximum potential difference between the electrodes, $I^{\max}_{\text{p.r.}}$ is the maximum current generated between the electrodes, $U^{*}_{\text{p.r.}}$ is the potential difference corresponding to the value of $I^{\max}_{\text{p.r.}}$, $N_{\text{p.r.}}$ is the number of ions reaching the electrodes, and $E_{\text{p.r.}}$ is the energy recorded by the calorimeter in the polar region).

The occurrence of luminous spots on the dipole surface in small magnetic fields and results of measurements by the equatorial calorimeter indicate that a considerable portion of the explosive plasma penetrates into lower latitudes outside the zone of recording by the polar calorimeter and the electrodes.

Conclusions. The experiments performed made it possible to develop a procedure for simulating the dynamics of development of a space explosion in a homogeneous magnetic field in the quasitrapping mode at $L \approx 2$ under laboratory conditions.

The main characteristic stages of the process are determined, beginning with the moment of formation of a three-dimensional magnetic cavity, which resembles a magnetic trap bent toward the poles, and ending with the stage of rather slow floating or drift of meridionally elongated plasma jets in a direction away from the dipole.

In some jets, the trapped plasma with a concentration of up to 10^{12} cm^{-3} existed for a long time (20 μsec and more).

For the chosen parameter ε_B, the stage of effective deceleration of the cloud by the magnetic field approaches but does not reach the maximum possible (for spatial scales) value of R_B because of the development of instability and subsequent strong structuring of the external boundary of the plasma.

Thus, the general energy balance in the system can be represented as follows. At the first stage, the cloud transfers 50–60% of its initial energy to the magnetic field. This energy can be partly expended in displacement of the diamagnetic cavity into the weak field region and additional acceleration of the plasma as whole, which is suggested by the occurrence of polarizing potentials and short-circuit longitudinal currents. The other part (about 15%) is released in the polar regions as losses of the kinetic energy of the ions.

From results of the experiments it follows that with increase of the parameter æ (with magnetic field reduction), the boundary of plasma reflection approaches the dipole surface, but the amount of energy supplied to the polar region decreases strongly, i.e., the efficiency of plasma trapping in the magnetic trap reduces appreciably. This phenomenon is of considerable interest because it is related to plasma injection at small heights $L \approx 1.1$–1.5, which is of practical importance to the space weather forecast and requires detailed investigation.

This paper was performed within the framework of the project "Space Experiment in a Laboratory" (Contract No. 09/31-00) and Federal Target Scientific and Engineering Program "Basic Space Research" [Grant No. 101-09(00)-P].

REFERENCES

1. J. Zinn, H. Hoerlin, and A. G. Petschek, "The motion of bomb debris following the starfish test," in: B. M. McCormac (ed.), *Radiation Trapped in the Earth's Magnetic Field*, Reidel Publ. Co., Dordrecht (1966), pp. 671–692.
2. E. L. Stupitskii, "Magnetospheric nuclear explosion," in: *Physics of Nuclear Explosions* [in Russian], Vol. 1, Nauka, Moscow (1997), pp. 398–413.
3. P. A. Bernhardt, R. A. Roussel-Dupre, M. B. Pongratz, et al. "Observations and theory of the AMPTE magnetotail barium releases," *J. Geophys. Res.*, **92**, No. A6, 5777–5794 (1987).
4. S. A. Nikitin and A. G. Ponomarenko, "Dynamics and spatial boundaries of retardation of the plasma cloud of an explosion in a dipole magnetic field," *Prikl. Mekh. Tekh. Fiz.*, **34**, No. 6, 3–10 (1993).
5. Yu. P. Zakharov, A. M. Orizhich, and A. G. Ponomarenko, *Laser Plasma and Laboratory Simulation of Nonstationary Space Processes* [in Russian], Inst. of Theor. and Appl. Mech., Sib. Div., Acad. of Sci. of USSR, Novosibirsk (1988).
6. S. A. Nikitin and A. G. Ponomarenko, "Energetic criteria for artificial magnetosphere formation," *Prikl. Mekh. Tekh. Fiz.*, **36**, No. 4, 3–7 (1995).
7. D. Winske, "Development of flute on expanding plasma clouds," *Phys. Fluids B*, **1**, No. 9, 1900–1910 (1989).
8. Yu. P. Zakharov, A. M. Orishich, A. G. Ponomarenko, and V. G. Posukh, "Experimental investigation of the efficiency of deceleration of expanding clouds of a diamagnetic plasma by a magnetic field," *Fiz. Plazmy*, **6**, No. 5, 674–678 (1986).
9. V. M. Antonov, Yu. P. Zakharov, A. V. Melekhov, et al., "Simulation of explosive-type cosmophysical phenomena in the laser experiments," in: Proc. of the Int. Symp. *Modern Problems of Laser Physics* (MPLP), Sib. Div., Russian Acad. of Sci., Novosibirsk (1996), pp. 359–363.
10. T. Muranaka, H. Nakashima, H. Uchimura, et al., "Analysis of exploding plasma behavior in a dipole magnetic field," *Jpn. J. Appl. Phys.*, **40**, Part 1, No. 2A, 824–831 (2001).
11. L. B. Gevorkyan, A. M. Orishich, A. G. Ponomarenko, et al., "Simulation of some astrophysical phenomena in laboratory experiments," in: *Aerophysical Investigations* (collected scientific papers) [in Russian], No. 6, Inst. of Theor. and Appl. Mech., Sib. Div., Acad. of Sci. of USSR, Novosibirsk (1976), pp. 192–196.